Synthesis and characterization of squaramide-based supramolecular polymers

Lauria, F.

CHAPTER 2

Supramolecular copolymerization of oxo- and thiosquaramide monomers

2.1 Abstract

In polymer chemistry, the formation of well-defined polymer microstructures can be modulated by the copolymerization of two or more monomers through covalent bond formation. This concept applied to the field of supramolecular polymers is still in its infancy with only several examples providing insight into the features of the monomers necessary for their co-assembly and methods to enable their characterization. Non-covalent interactions such as π-π interactions and hydrogen bonding have been used to drive the formation of supramolecular copolymers, with amides being largely used to provide directional interactions in the assemblies. In this chapter, the potential of an underrepresented hydrogen bonding unit, squaramide, to be used for supramolecular copolymerization will be examined. We previously showed that oxosquaramides self-assemble in a head-to-tail fashion whereas thiosquaramides stack upon one another. The potential for their copolymerization through the use of distinct hydrogen bond-acceptor moieties, namely oxo- and thio-derivatives will be explored. In particular, I will first examine the self-assembly properties of the individual monomers into supramolecular polymers and determine conditions for their copolymerization. Spectroscopic and imaging techniques at the nanoscale show progressive fiber shortening and a decreased fiber persistence length providing a handle to tune the supramolecular polymerization behavior of oxosquaramides. To further elucidate the copolymerization behavior of oxo- and thiosquaramide monomers, a fluorescent Cyanine 3 (Cy3) dye-labelled oxo-squaramide and Cyanine 5 (Cy5) dye-labelled thiosquaramide monomers were synthesized. The fluorescence and UV-vis measurements show fluorescence resonance energy transfer (FRET) from oxo-squaramide-Cy3 to thio-squaramide-Cy5 suggestive of the supramolecular copolymerization in a block structure.

2.2 Introduction

The structural complexity of biological systems over several length scales remains an inspiration for the design of functional polymer materials.[1] The sequence-controlled polymerization of biological macromolecules, such as nucleic acids and proteins, leads to a well-defined arrangement of biomolecular building blocks with hierarchical structure and function.[2] Conversely, in the last several decades the field of covalent polymers has used copolymerization to tune their properties to obtain specific properties and function.[3, 4] Two or more monomers can be combined within the same polymer using living,[5] controlled radical,[6] and ring opening metathesis polymerization[7] using techniques to gain control over their length, structure and composition. When coupled with monomers of different reactivities[2, 8] copolymers with alternating, periodic, and blocky structures can be prepared providing a range of structural diversity and vast differences in the physical properties of the resultant materials.

The concept of supramolecular copolymerization[9-16] is a more recent addition to the supramolecular polymer field consistent with the growing knowledge of monomer assembly and their polymerization mechanisms. Similar to covalent polymers, the aim is to be able to achieve the properties that cannot be accessed through single component systems. However, the structural design of the monomers complexity of the copolymer formation and mechanistic features still faces several challenges.[17, 18] Nevertheless, supramolecular copolymers that rely on electrostatic, hydrogen bonding,[19] transition metal,[20, 21] or π-π interactions for their formation have been reported.[22] For example, copolymers based on distinct hydrogen bond acceptor groups, oxygen or sulfur, were demonstrated for 1,3,5-benzenetricarboxamides (BTA).[23] Although thio-BTA forms less directional hydrogen bonds, the two monomers can self-assemble independently into one-dimensional long fibers following a cooperative mechanism. When the monomers are co-assembled, random copolymers were observed. Moreover, George and coworkers demonstrated the potential for sequence controlled supramolecular polymerization using two component systems showing pathway complexity.[24] In this study the kinetic and thermodynamic pathways in the self-assembly of core-substituted naphthalene diimide monomers (NDI) were exploited to control the formation of various random, block copolymers and self-sorted supramolecular polymers. Despite recent examples that provide analysis and insight into supramolecular monomers that enable copolymerization, there still remains much to understand regarding the

existing repertoire of self-assemblies motifs in this area and the potential to control the microstructural features of the polymers especially in aqueous medium remains untapped.

When hydrogen bonds are employed in the molecular designs of supramolecular monomers,[25-28] amides and ureas[29] are attractive because of their ditopic nature. We recently demonstrated the utility of the squaramide unit to provide directional hydrogen bonding in a ditopic manner to drive the formation of supramolecular polymers in water through their self-assembly in a head-to-tail fashion.[30] When we thionate the monomer, replacing the oxygens with sulfur atoms, the monomer self-assembly mode is altered to a stacking mode.[31] Because of capacity of the squaramide to engage in hydrogen bonding and stacking interactions, we became interested to understand if the individual self-assembly modes of the oxo- and thiosquaramide monomers could be affected in the presence of each other, or if co-assembly occurs. Thus, in this chapter, the protocols to facilitate and evaluate the supramolecular polymerization of the individual oxo- and thiosquaramide monomers, and their copolymerization at various molar ratios is studied.

2.3 Results and discussion

The design of the oxosquaramide (**1**) and thiosquaramide monomers (**2**) involves two ditopic hydrogen-bonding squaramide units within the hydrophobic alkyl chains, surrounded by two oligo(ethylene glycol) methyl ether chains for their self-assembly in water (**Figure 2.1**). **1** was synthesized as previously described by Talens *et al.*[30] and **2** was obtained by the thionation reaction of **1** in presence of an excess of P_4S_{10}·pyridine complex (23 eq) in a yield of 30%. Exclusive thionation of squaramide moieties was obtained at room temperature as previously reported for Lawesson's agent in the preparation of *N*-(benzoyloxy)thioamide.[32]

In order to track the mixing of the two monomers at the molecular level, a fluorescently-labelled thiosquaramide monomer **12** was synthesized that is asymmetrically outfitted with a sulfo-Cyanine dye (sulfo-Cy5), in addition to a previously reported oxosquaramide monomer **11** (sulfo-Cy3).[33] The two fluorescently-labelled monomers were synthesized following a similar synthetic procedure (**Scheme 1**). Specifically, **12** was obtained firstly by thionation of compound **9**, before being conjugated to sulfo-Cy5 dye (**Scheme 1**). The synthesis of asymmetric fluorescently-labelled molecules was performed starting with O-(2-azidoethyl)undecaethylene glycol that was

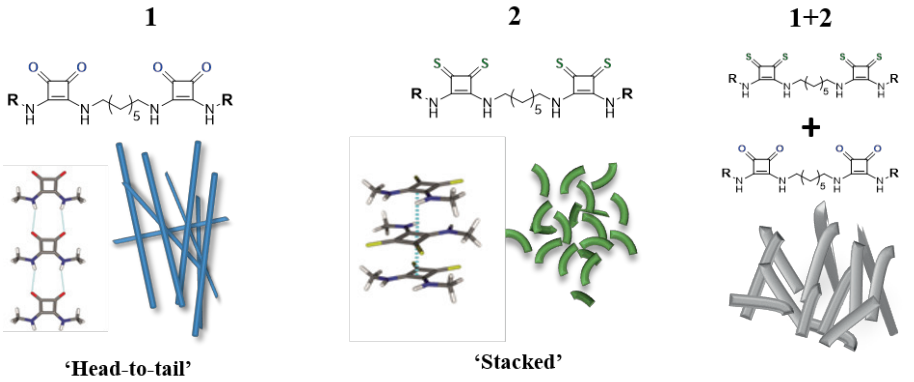

Figure 2.1 Oxosquaramide (**1**) and thiosquaramide (**2**) monomers, supramolecular polymers and copolymers. Oxosquaramide bolaamphiphiles (**1**) self-assemble into rigid nanofibers (*left*), whereas thiosquaramides (**2**) self-assemble into shorter nanorods (*center*) because of their different self-assembly mode. The self-assembly of the two monomers (**1+2**, right) results in the formation of copolymers with the characteristics of both individual polymers.

converted to amine by catalytic hydrogenation using Et_3SiH on Pd/C. After Boc-protection of the amine, the hydroxyl group of undecaethylene glycol was activated with CDI and subsequently, coupled with N-Cbz-1,10-decanediamine to obtain **7**. The deprotection of the Cbz group and coupling with squaric ester resulted in squaramide amphiphile **8**. The asymmetric oxosquaramide **9** was synthesized through conjugation of **8** with another squaramide-based amphiphile functionalized with a mono-Boc protected heptanediamine **5**. To obtain the fluorescently-labelled oxosquaramide **11**, **9** was coupled with sulfo-Cyanine 3 N-hydroxysuccinimidyl ester. The Cy5-labelled thiosquaramide **12** was prepared after the thionation of **9** by coupling sulfo-Cyanine 5 N-hydroxysuccinimidyl ester. Both compounds were purified by high performance liquid phase chromatography on reverse phase C18 columns and characterized.

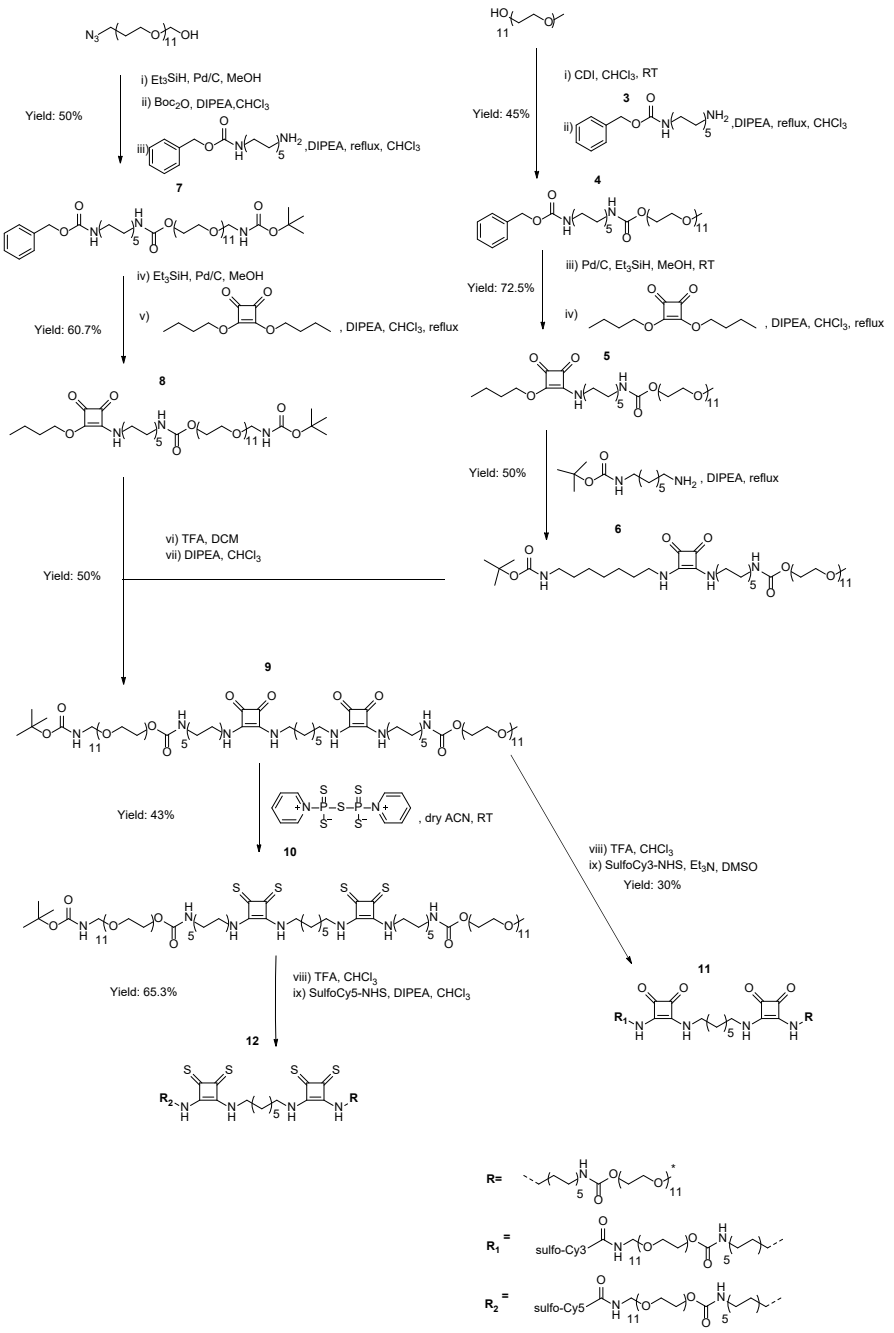

Scheme 1 Synthetic scheme of sulfo-Cy3 and sulfo-Cy5-labelled oxo- and thiosquaramide monomers (**11** and **12**).

Prior to the co-assembly of the oxo- and thiosquaramide monomers, insight into the self-assembly of the individual monomers at the molecular level and their polymerization mechanisms was carried out. The UV-vis spectra of **1** in water displays two bands at 329 and 255 nm that correspond to π-π* of hydrogen bond donor N-H and n-π* transition of C=O hydrogen bond acceptor, respectively, in their aggregated state **(Figure 2.2a).** According to Kasha's theory,[34] these blue and red shifted transitions (H- and J- bands) of oxosquaramide are due to the in-line and parallel orientation of transition dipole moments within the squaramide moieties upon self-assembly in a head-to-tail hydrogen bonding orientation as determined from time-dependent density functional theory calculations (TD-DFT) calculations.

Self-assembly of **2** in water resulted in opposite trends as observed in the UV-vis spectroscopy (**Figure 2.2b).** More specifically, the thionation of the squaramide moieties results in the formation of two bands at 272 and 363 nm. According to Kasha's theory, the blue-shifted transition in the UV-vis profile is in line with the formation of H-type aggregates as consequence of the parallel orientation of the transition dipole moments. To further evaluate the thionation of thiosquaramide on the self-assembly in water, critical aggregation concentration (CAC) was determined by SLS. The CAC of **2** was determined by preparing various solutions in the concentration range of 100 μM and 10 nM and was calculated from the inflection point of the scattering intensity as a function of concentration range. The CAC was comparable to the value previously determined for **1** (8×10^{-5} M, **Figure S2.4**), despite its distinct self-assembly mode.[30]

To investigate the polymerization mechanisms of **1** and **2**, conditions that would enable depolymerization of the polymers was necessary to determine. Thermal denaturation and titration with a 'good' solvent were examined to induce their self-assembly. Thermal denaturation of **1** was first attempted by recording individual UV-vis spectra from 20 to 65 °C (SI **Figure S2.1**). Despite the disappearance of red shifted band (329 nm) at higher temperatures, the blue shifted band (255 nm) was maintained and only a slight increase in the monomer band (310 nm) was observed. As previously reported,[30] depolymerization of **1** was achieved by the addition of very strong hydrogen bond disrupting solvent ('good' solvent) hexafluorisopropanol (HFIP) to a supramolecular polymer in 'poor' solvent (i.e. water). Depolymerization through the titration with HFIP (hexafluoroisopropanol) results in the gradual loss of the blue (255 nm) and red shifted transition (329 nm) and an increase

of the monomer band at 310 nm (**Figure 2.2a).** To confirm depolymerization of the monomers, NMR spectroscopy and static light scattering (SLS) were performed. NMR spectra of the aggregated (in D_2O) and depolymerized states (in HFIP-d_2) were analyzed. While the NMR spectrum of **1** in D_2O (**Figure S2.6**) suggests aggregation of the monomers that is still present up to 65 °C, in HFIP-d_2 (**Figure S2.5**) a well resolved spectrum is observed and is indicative of the depolymerized state. These results were further supported by SLS measurements, where the scattered light intensities of the aggregated and depolymerized states were analyzed in water and HFIP, respectively. High counts rates for **1** in water were observed in comparison to that of HFIP suggesting the presence of self-assembled aggregates in water and monomer species in HFIP (**Table S1**).

To further examine the solvent-induced depolymerization of **2**, UV-vis spectra in different organic solvents were recorded (**Figure S2.2**). In contrast to **1**, all UV-vis profiles of **2** displayed an increase in the bands at 350 and 380 nm, except for THF (**Figure S2.2**). The UV-vis spectra of **2** in THF showed two bands at 235 and 325 nm that are blue-shifted in comparison to the transitions observed in in the presence of water. In order to support the observed UV-vis transitions, atomic force microscopy was performed on drop-casted samples of **2** in water, THF and HFIP. Aggregation was observed in water and HFIP, but not in THF (**Figure S2.2**). Further confirmation of the disassembly of the polymers was evaluated by ^{1}H NMR spectroscopy. The NMR spectrum of **2** in THF-d8, is well resolved suggesting of complete depolymerization (**Figure S2.7**). Conversely, the ^{1}H NMR in D_2O displays a broad signal at 3.5 ppm that is still present up to 65 °C and indicates that **2** retains its self-assembled state (**Figure S2.8**). The depolymerization of **2** in THF was further supported by SLS, where the scattered light intensities of the aggregated and depolymerized states were analyzed in water and THF, respectively. Compared to their respective solvent controls, no scattering species were detected in THF while in water high scattered light intensities are recorded. Hence, these results suggest a lack of aggregation in THF.

Once the conditions for depolymerization were established, UV-vis titrations were performed for **1** and **2**, using co-solvents HFIP and THF as denaturants, respectively, to gain insight into the differences in the thermodynamic parameters associated with their aggregation. In the case of molecule **1** (c = 30 μM), 10 % of HFIP (v/v) was required to achieve depolymerization using disappearance of the band at 329 nm. The same approach was performed for

molecule **2** (c = 30 µM) (363 nm) and THF that was added until (10 % (v/v)) until no further changes in the absorption were observed.

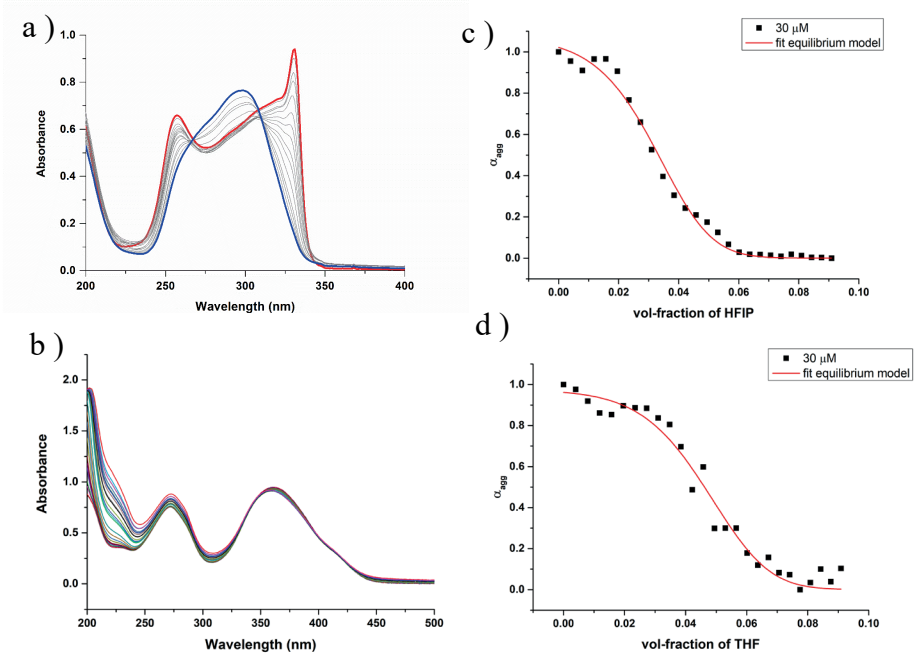

Figure 2.2 UV-vis titrations with the addition of a co-solvent to the squaramide monomer in water: (a) **1** (c=30 µM) with HFIP; (b) **2** (30 µM) with THF; Plot of α_{agg} as function of volume fraction of co-solvent for (c) **1** at 329 nm; (d) **2** at 363 nm.

The aggregated fraction of supramolecular polymers **1** and **2** were determined using the absorbances at 329 and 363 nm, respectively, (**Figure 2.2 c-d**) and plotted as a function of solvent volume fraction. The depolymerized state of **1** and **2** was observed at different volume fractions of good solvent: while **1** depolymerizes at 6 vol % of HFIP, **2** required more THF (8 vol%) indicative of a more stable polymer. To determine the thermodynamic parameters for the supramolecular polymerization of the monomers (ΔG**,** m and σ, **Table S1**), the curves were fit with the solvent denaturation model by Korevaar *et al.*[35, 36] From the fitted data, the cooperativity parameters, σ, of monomers **1** and **2** were was less than 1, indicating that the monomers polymerize according to a cooperative mechanism. Moreover, although monomer **2** self-assembles in a stacked mode, the cooperativity parameter (σ = 0.06) was found to be less than that obtained for **1** (σ = 0.78). Additionally, comparable ΔG values were

obtained with both monomers **1** (-34 kJ/mol) and **2** (-35 kJ/mol), indicating a similar stability, despite their distinct self-assembly modes.

Conversely, in our previous publication, both of the monomers were titrated with the same solvent (CH_3CN) and the depolymerized state of **1** and **2** was reached with 24.5 vol % and 33.3 vol% of CH_3CN respectively.[31] Moreover, some differences were observed also in the thermodynamic parameters of polymerization mechanism. Specifically, cooperativity parameter (σ) of **1** (0.013) is an order magnitude smaller compared to **2** (0.610).[31] However, both of these values are within the calculated error.

2.3.1 Oxo- and thiosquaramide supramolecular copolymers

To better understand if the distinct self-assembly modes of the squaramide unit can support the formation of supramolecular copolymers, studies that examine the extent of their copolymerization were pursued. Using the information gained by dissolving the monomers in various organic solvents and evaluating their dissolution in the earlier section, a protocol for the mixing of both supramolecular monomers was developed. In this protocol, **1** was dissolved in HFIP and **2** in THF, and the organic solvent was removed by a stream of N_2. After the rehydration with water, the monomers were mixed in the appropriate molar ratio as shown in **Figure 2.4a.**

The extent of monomer mixing at the molecular level was first examined by UV-vis and fluorescence spectroscopy. Because of the distinct UV-vis profiles of **1** and **2** that are due to their head-to-tail and stacked self-assembly configurations, respectively, insight into the microstructure of the copolymers can be obtained if they co-assemble. At an equimolar ratio of **1** and **2**, UV-vis profiles shows that there is overlap of the individual spectra of the monomers indicating the retention of their transitions in self-assembled state (**Figure 2.4b)**. Moreover, at molar ratios (2:1 and 1:2) (**Figure 2.4c**), the UV-vis absorption spectra of the single monomers are still retained with the bands of the monomer in excess showing an increased intensity in comparison to the other monomer (**Figure 2.4c)**.

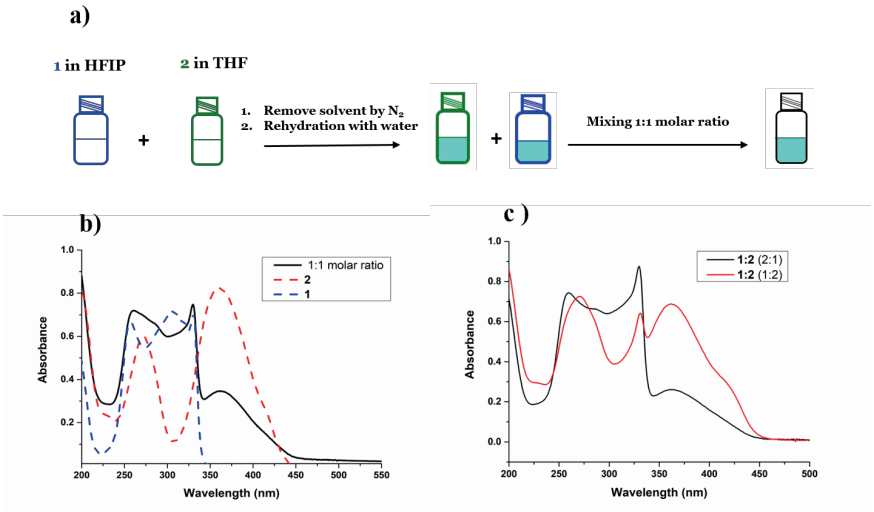

Figure 2.4 (a) Pictorial representation of the co-assembly protocol of **1** and **2** (b) UV-vis absorption spectra of the individual molecules, **1, 2** and copolymers a 1:1 molar ratio (c_{tot}= 30 µM each) (c) UV-vis absorption spectra of monomers **1** and **2** mixed in a 1:2 and 2:1 molar ratio to form supramolecular copolymers (c_{tot}= 30 µM, 1:1 molar ratio)

To further understand if monomers **1** and **2** undergo co-assembly or self-sorting under the developed mixing conditions, zeta potential and fluorescence resonance energy transfer (FRET) experiments were performed. Monomers **1** and **2** were conjugated to sulfo-Cy3 and sulfo-Cy5 dyes, respectively, as described above to execute FRET studies for gaining insight into the extent of their mixing. Zeta potential measurements were then used to confirm that the sulfo-Cy dye-labelled monomers can co-assemble with the native monomers. When **1** was mixed with 2 mol% of **11**, a more negative ζ potential value (-4.9±5.2 mV) was obtained in comparison to the native monomer (7.32±5.5 mV). The same trend was observed in the case of **2** mixed with 2 mol% of **12** (-8.57±4.53 mV), compared to the native monomer (-0.321±5.65 mV). These slight decrease in zeta potential suggests results co-assembly of the dye-labelled monomers with their non-labelled variants.

Once co-assembly of the dye-labelled monomers was confirmed, a FRET study was carried out on the various copolymer solutions. Copolymerization of the monomers can be followed by excitation of the sulfo-Cy3 donor at 550 nm that undergoes its energy transfer to a sulfo-Cy5 acceptor resulting in a measurable fluorescence signal at 670 nm**.** The individual monomers **1** and **2** were co-assembled with their respective fluorescent monomers **11** and **12** in

HFIP and THF, respectively, to ensure that a molecularly dissolved state is obtained. Subsequently, after the removal of the solvent under N_2 gas, the solution were rehydrated with water and immediately mixed in an equimolar ratio (total dye concentration: 2 mol%). **(Figure 2.5a)** As shown in the **Figure 2.5c,** the FRET experiment resulted an emission band at 670 nm confirming the co-assembly event when excited at 550 nm.

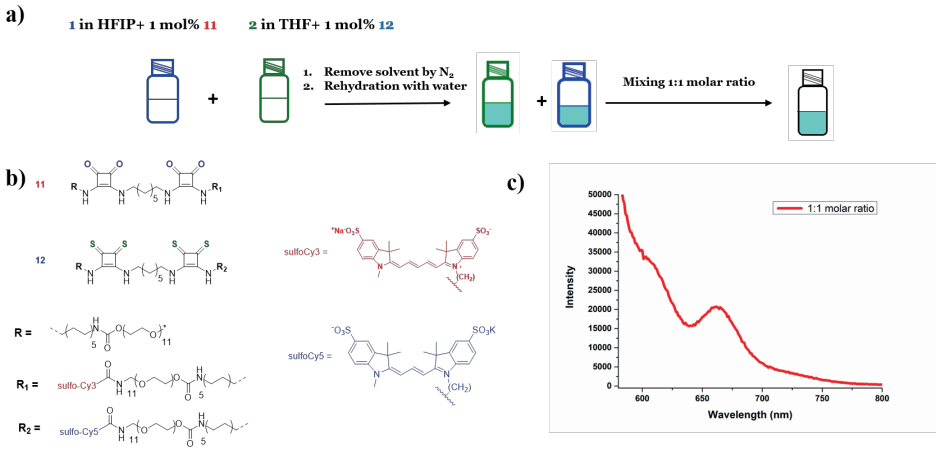

Figure 2.5 (a) Co-assembly protocol of **1** and **2** for FRET experiments (b) Chemical structures of squaramide monomer sulfo-Cy dye-conjugates (**11**) and (**12**) (c) Fluorescence emission spectrum of a solution containing an equimolar ratio of **1** and **2** with 2 mol% of **11** and **12** (2 mol% total dye concentration). Excitation wavelength 550 nm (sulfo-Cy3), Emission range 570-800 nm (sulfo-Cy5).

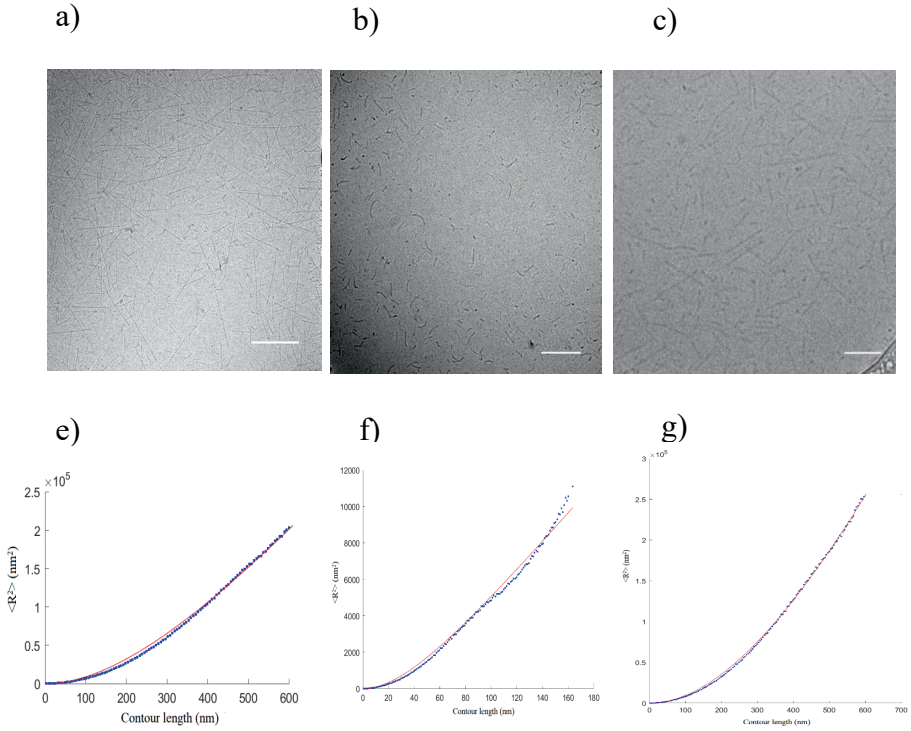

Figure 2.6 CryoTEM micrographs of squaramide-based supramolecular (co)polymers: (a) **1** (c=580 µM), scale bar: 100 nm; (b) **2** (c=580 µM), scale bar: 100 nm; (c) **1** and **2** in an equimolar ratio (c=580 µM), scale bar: 100 nm. End-to-end distance plots (R^2) as function of contour length for **1** (e), **2** (f) and copolymerization of **1** and **2** in an equimolar ratio (g) as obtained from the Easyworm software.

The copolymerization of **1** and **2** were demonstrated on the molecular level through various spectroscopies, but we sought to understand the consequence of their mixing on the aggregates at the nanoscale. Consequently, we performed cryo-EM measurements on the individual monomers (**1**) and (**2**) and their copolymers. While monomers of **1** self-assemble into high-aspect-ratio fibers, monomers of **2** self-assemble into more flexible nanorod-like structures that are approximately 5-times shorter in length. When both monomers are copolymerized, cryoEM micrographs show the formation of nanofibers with a shorter length compared to **1**, but longer than **2**. Image analysis using the Easyworm software[37] was performed to quantify various fiber properties. The mean square of the end-to-end distance $< R^2 >$ is measured as a function of contour length of the fibers (ℓ) (Figures **2.6d, e** and **f**) and the persistence length of the fibers (P_l) was calculated using the worm-

like chain model (WLC). While **1** and **2** display a P_l value of 581 ± 76 nm and 47 ± 4 nm respectively, the mixing of **1** and **2** results in a decrease in fiber length relative to **1** of 282 ± 16 nm. Moreover, using P_l, bending rigidity of the nanofibers (κ) was determined. Monomers **1** and **2** display a bending rigidity of (2.4 ± 0.3) x 10^{-27} N·m^2 and (1.9± 0.2) x 10^{-28} N·m^2 respectively, and their equimolar mixture results in a value of (1.16± 0.07) x 10^{-27} N·m^2. These preliminary results demonstrate that the mixing of monomers **1** and **2** prior to their self-assembly results in structural changes to the properties of the formed supramolecular polymers with respect to their length and bending rigidity. Modulation of the oxosquaramide assemblies is likely due to the stacking tendency of the thiosquaramide synthon and its less directional hydrogen bonding character. To further understand the copolymer microstructure, superresolution microscopy experiments would need to be performed using the dye-labelled monomers. A similar approach was recently taken by George and coworkers using structured illumination (SIM) to visualize the supramolecular copolymer microstructure of naphthalene diimide derivatives (NDI).[24] Furthermore, to better understand the potential for microstructural control over the polymers, ratios beyond (1:2 and 2:1) should be considered.

2.4 Conclusions

In this chapter, the capacity of two monomers with distinct self-assembly modes to form copolymers was examined. A molecularly dissolved state was achieved for both monomers in different solvents prior to their mixing; HFIP is a good solvent for **1**, while THF is a good solvent for **2**. Solvent denaturation studies using the determined good solvents showed that a cooperative process is followed for their respective self-assemblies. On co-assembly, UV-vis spectra of an equimolar ratio of **1** and **2** reflected the profiles of the individual monomers, based on the retention of their bands. FRET experiments in the presence of sulfo-Cyanine labelled monomers of **1** and **2** are suggestive of co-assembly due to the presence of an emission band at 670 nm. Investigation of the supramolecular copolymer morphology by cryoTEM that showed shorter fibers with a decreased persistence length compared to **1**. In conclusion, since oxo- and thiosquaramide maintain their independent assemblies when mixed, this approach may be pursued to control the copolymerization of squaramide-based monomers in water. Moreover, to further understand the formed co-polymer microstructure through self-assembly, superresolution microscopy experiments using the dye-labelled monomers would need to be performed.

References

1. Leibfarth, F. A.; Mattson, K. M.; Fors, B. P.; Collins, H. A.; Hawker, C. J., External regulation of controlled polymerizations. *Angew. Chem. Int. Ed. Engl* **2013,** *52*, 199-210.
2. Lutz, J. F.; Ouchi, M.; Liu, D. R.; Sawamoto, M., Sequence-controlled polymers. *Science* **2013,** *341*, 1238149, 1-8.
3. Lutz, J.-F.; Lehn, J.-M.; Meijer, E. W.; Matyjaszewski, K., From precision polymers to complex materials and systems. *Nat. Reviews Mater.* **2016,** *1,*1-14.
4. Feng, H.; Lu, X.; Wang, W.; Kang, N. G.; Mays, J. W., Block copolymers: synthesis, self-assembly, and applications. *Polymers (Basel)* **2017,** *9*, 494, 1-31.
5. Szwarc, M., 'Living' polymers. *Nature* **1956,** *178*, 1168-1169.
6. Ouchi, M.; Terashima, T.; Sawamoto, M., Transition metal-catalyzed living radical polymerization: toward perfection in catalysis and precision polymer synthesis. *Chem. Rev.* **2009,** *109*, 4963-5050.
7. Bielawski, C. W.; Grubbs, R. H., Living ring-opening metathesis polymerization. *Progr. Polym. Sci.* **2007,** *32*, 1-29.
8. Satoh, K.; Ishizuka, K.; Hamada, T.; Handa, M.; Abe, T.; Ozawa, S.; Miyajima, M.; Kamigaito, M., Construction of sequence-regulated vinyl copolymers via iterative single vinyl monomer additions and subsequent metal-catalyzed step-growth radical polymerization. *Macromolecules* **2019,** *52*, 3327-3341.
9. Thota, B. N. S.; Lou, X.; Bochicchio, D.; Paffen, T. F. E.; Lafleur, R. P. M.; van Dongen, J. L. J.; Ehrmann, S.; Haag, R.; Pavan, G. M.; Palmans, A. R. A.; Meijer, E. W., Supramolecular copolymerization as a strategy to control the stability of self-assembled nanofibers. *Angew. Chem. Int. Ed. Engl.* **2018,** *57*, 6843-6847.
10. Ahlers, P.; Fischer, K.; Spitzer, D.; Besenius, P., Dynamic light scattering investigation of the kinetics and fidelity of supramolecular copolymerizations in water. *Macromolecules* **2017,** *50*, 7712-7720.
11. Albertazzi, L.; van der Veeken, N.; Baker, M. B.; Palmans, A. R.; Meijer, E. W., Supramolecular copolymers with stimuli-responsive sequence control. *Chem. Commun. (Camb)* **2015,** *51*, 16166-16168.
12. Engel, S.; Spitzer, D.; Rodrigues, L. L.; Fritz, E. C.; Strassburger, D.; Schonhoff, M.; Ravoo, B. J.; Besenius, P., Kinetic control in the temperature-dependent sequential growth of surface-confined supramolecular copolymers. *Faraday Discuss.* **2017,** *204*, 53-67.

13. Hendrikse, S. I. S.; Su, L.; Hogervorst, T. P.; Lafleur, R. P. M.; Lou, X.; van der Marel, G. A.; Codee, J. D. C.; Meijer, E. W., Elucidating the ordering in self-assembled glycocalyx mimicking supramolecular copolymers in Water. *J. Am. Chem. Soc.* **2019,** *141*, 13877-13886.
14. van Buel, R.; Spitzer, D.; Berac, C. M.; van der Schoot, P.; Besenius, P.; Jabbari-Farouji, S., Supramolecular copolymers predominated by alternating order: theory and application. *J. Chem. Phys.* **2019,** *151*, 014902, 1-17.
15. Ten Eikelder, H. M. M.; Adelizzi, B.; Palmans, A. R. A.; Markvoort, A. J., Equilibrium model for supramolecular copolymerizations. *J. Phys. Chem. B* **2019,** *123*, 6627-6642.
16. Das, A.; Vantomme, G.; Markvoort, A. J.; Ten Eikelder, H. M. M.; Garcia-Iglesias, M.; Palmans, A. R. A.; Meijer, E. W., Supramolecular copolymers: structure and composition revealed by theoretical modeling. *J. Am. Chem. Soc.* **2017,** *139*, 7036-7044.
17. Hirst, A. R.; Smith, D. K., Two-component gel-phase materials--highly tunable self-assembling systems. *Chemistry* **2005,** *11*, 5496-5508.
18. Makam, P.; Gazit, E., Minimalistic peptide supramolecular co-assembly: expanding the conformational space for nanotechnology. *Chem. Soc. Rev.* **2018,** *47*, 3406-3420.
19. Felder, T.; de Greef, T. F.; Nieuwenhuizen, M. M.; Sijbesma, R. P., Alternation and tunable composition in hydrogen bonded supramolecular copolymers. *Chem. Commun. (Camb)* **2014,** *50*, 2455-2457.
20. Frisch, H.; Nie, Y.; Raunser, S.; Besenius, P., pH-regulated selectivity in supramolecular polymerizations: switching between Co- and homopolymers. *Chemistry* **2015,** *21*, 3304-3309.
21. Frisch, H.; Unsleber, J. P.; Ludeker, D.; Peterlechner, M.; Brunklaus, G.; Waller, M.; Besenius, P., pH-Switchable ampholytic supramolecular copolymers. *Angew. Chem. Int. Ed. Engl.* **2013,** *52*, 10097-10101.
22. Gorl, D.; Zhang, X.; Stepanenko, V.; Wurthner, F., Supramolecular block copolymers by kinetically controlled co-self-assembly of planar and core-twisted perylene bisimides. *Nat. Commun.* **2015,** *6*, 7009, 1-8.
23. de Windt, L. N. J.; Kulkarni, C.; Ten Eikelder, H. M. M.; Markvoort, A. J.; Meijer, E. W.; Palmans, A. R. A., Detailed approach to investigate thermodynamically controlled supramolecular copolymerizations. *Macromolecules* **2019,** *52*, 7430-7438.
24. Sarkar, A.; Sasmal, R.; Empereur-Mot, C.; Bochicchio, D.; Kompella, S. V. K.; Sharma, K.; Dhiman, S.; Sundaram, B.; Agasti, S. S.; Pavan, G. M.; George, S. J., Self-Sorted, random, and block supramolecular copolymers via

sequence controlled, multicomponent self-Assembly. *J. Am. Chem. Soc.* **2020,** *142*, 7606-7617.
25. Pinault, T.; Andrioletti, B.; Bouteiller, L., Chain stopper engineering for hydrogen bonded supramolecular polymers. *Beilstein J. Org. Chem.* **2010,** *6*, 869-875.
26. Folmer, B. J. B.; Sijbesma, R. P.; Versteegen, R. M.; van der Rijt, J. A. J.; Meijer, E. W., Supramolecular polymer materials: chain extension of telechelic polymers using a reactive hydrogen-bonding synthon. *Adv. Mater.* **2000,** *12*, 874-878.
27. Mes, T.; Smulders, M. M. J.; Palmans, A. R. A.; Meijer, E. W., Hydrogen-bond engineering in supramolecular polymers: polarity influence on the self-assembly of benzene-1,3,5-tricarboxamides. *Macromolecules* **2010,** *43*, 1981-1991.
28. Yan, X.; Li, S.; Pollock, J. B.; Cook, T. R.; Chen, J.; Zhang, Y.; Ji, X.; Yu, Y.; Huang, F.; Stang, P. J., Supramolecular polymers with tunable topologies via hierarchical coordination-driven self-assembly and hydrogen bonding interfaces. *PNAS* **2013,** *110*, 15585-15590.
29. Isare, B.; Pensec, S.; Raynal, M.; Bouteiller, L., Bisurea-based supramolecular polymers: From structure to properties. *Comptes Rendus Chimie* **2016,** *19*, 148-156.
30. Saez Talens, V.; Englebienne, P.; Trinh, T. T.; Noteborn, W. E.; Voets, I. K.; Kieltyka, R. E., Aromatic gain in a supramolecular polymer. *Angew. Chem. Int. Ed. Engl.* **2015,** *54*, 10502-10506.
31. Saez Talens, V.; Davis, J.; Wu, C.-H.; Wen, Z.; Lauria, F.; Gupta, K. B. S. S.; Rudge, R.; Boraghi, M.; Hagemeijer, A.; Trinh, T. T.; Englebienne, P.; Voets, I. K.; Wu, J. I.; Kieltyka, R. E., Thiosquaramide-based supramolecular polymers: aromaticity gain in a switched mode of self-assembly. *J. Am.Chem. Soc.* **2020**, *142*, 47, 19907-19916.
32. Wang, L.; Phanstiel, Synthesis of N-(hydroxy)amide- and N-(Hydroxy)thioamide-containing peptides. *J.Org. Chem.* **2000,** *65*, 1442-1447.
33. Saez Talens, V.; Arias-Alpizar, G.; Makurat, D. M. M.; Davis, J.; Bussmann, J.; Kros, A.; Kieltyka, R. E., Stab2-Mediated clearance of supramolecular polymer nanoparticles in zebrafish embryos. *Biomacromolecules* **2020,** *21*, 1060-1068.
34. Kasha, M.; Rawls, H. R.; Ashraf El-Bayoumi, M., The exciton model in molecular spectroscopy. *Pure Appl. Chem.* **1965,** *11*, 371-392.
35. Korevaar, P. A.; Schaefer, C.; de Greef, T. F. A.; Meijer, E. W., Controlling chemical self-assembly by solvent-dependent dynamics. *J. Am. Chem. Soc.* **2012,** *134*, 13482-13491.

36. Goldstein, R. F.; Stryer, L., Cooperative polymerization reactions. Analytical approximations, numerical examples, and experimental strategy. *Biophys. J.* **1986,** *50*, 583-599.
37. Lamour, G.; Kirkegaard, J. B.; Li, H.; Knowles, T. P. J.; Gsponer, J., Easyworm: an open-source software tool to determine the mechanical properties of worm-like chains. *Source Code Biol. Med.* **2014,** *9*, 16, 1-6

SUPPORTING INFORMATION

2.6 Materials and methods

2.6.1 Materials

All reagents and chemicals were purchased from Sigma Aldrich and Acros Organics and used without further purification. Deuterated chloroform was obtained from Euriso-top and Milli-Q water was employed for all experiments. For the hydrogenation reaction, acetonitrile was dried with molecular sieves (3 Å, 20 % w/v), whereas for the thionation reaction anhydrous acetonitrile purchased from Sigma Aldrich was employed.

S2.6.2 Instrumentation

Compounds were either purified by silica gel column chromatography or on X1 flash chromatography system equipped with a C18 column from Grace Reveleris using a gradient of H_2O/CH_3CN. ^{1}H-NMR and ^{13}C spectra were obtained on a Bruker (300 MHz) or Bruker DMX-400 (400 MHz). LC-MS analysis was performed on a Finnigan Surveyor HPLC system equipped with a Gemini C18 50 x 4.60 mm column (UV detection at 254 and 214 nm) coupled to a Finnigan LCQ Advantage Max mass spectrometer with ESI. Thiosquaramide-containing molecules were detected using wavelengths of 384 and 228 nm. For the mobile phase, a gradient of 10-90% of CH_3CN/H_2O with 0.1% trifluoroacetic acid over 13.5 minutes was used. MALDI-TOF-MS spectra were obtained on a Bruker Microflex LRF mass spectrometer in reflection positive mode using α-cyano-4-hydroxycinnamic acid with a laser power of 30%. UV-vis measurements were performed on a Cary 300 UV-vis spectrophotometer using a quartz cuvette of 1 cm path length. DLS measurements were carried out using a Malvern Zetasizer Nano ZS ZEN3500 equipped with a laser of 633 nm and a scattering angle of 173°. Atomic force microscopy (AFM) images were recorded in tapping mode on a Veeco-Bruker Multimode AFM with a Nanoscope IIIa controller at room temperature. The AFM tips used were Oltespa Opus probes with a reflex aluminium coating, with a nominal spring constant of 2 N/m, a nominal resonance frequency of 70 kHz and a tip radius of 7 nm. The images were processed using Nanoscope software. Fluorescence experiments were recorded on an Infinite M1000 Pro Tecan plate reader with a black background 96-well plate.

Cryo-TEM images were collected using a Tecnai F12 (FEI Company, The Netherlands) equipped with a field emission gun operating at 120 keV using a Gatan UltraScan charge-couple device (CCD) camera (Gatan company, Germany) with a defocus between −6 and −9 μm.

2.6.3 Synthetic schemes

Synthesis of squaramide-based bolaamphiphiles

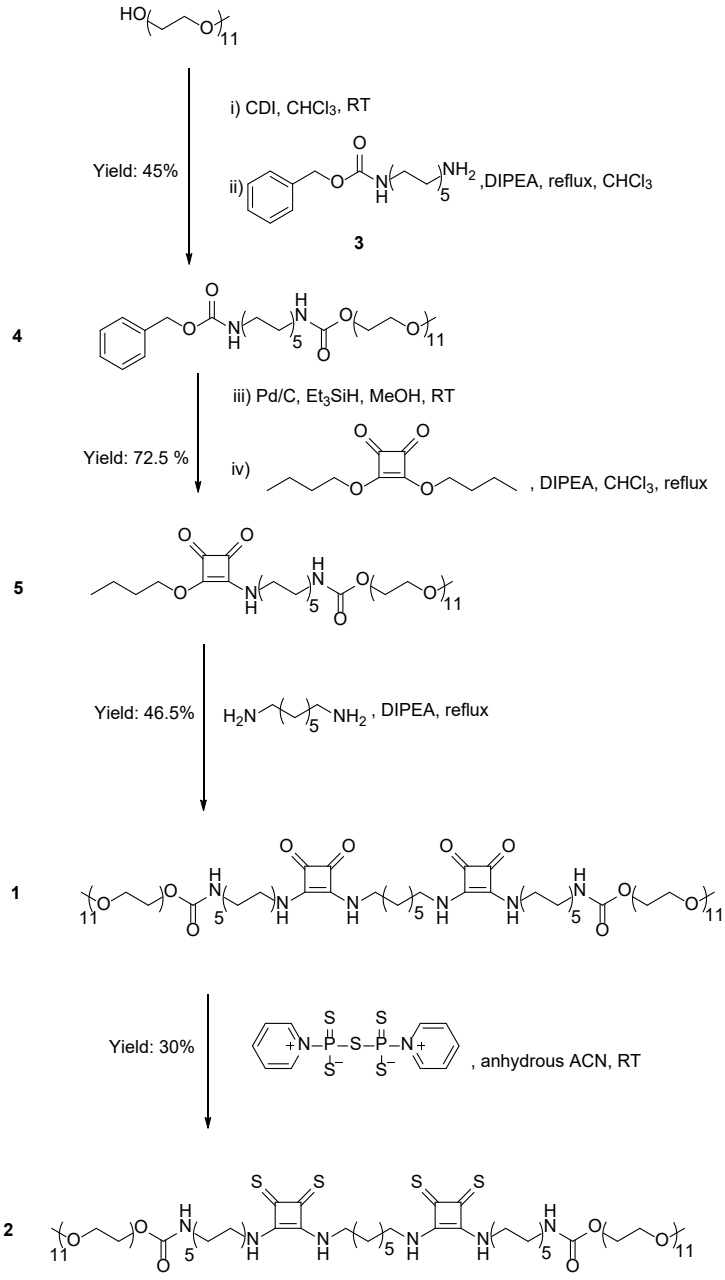

Synthesis of 3

1,10-diaminodecane (10 g, 58.03 mmol) was dissolved in DCM (100 mL) and cooled down to 0 °C. Benzyl chloroformate (1.65 ml, 11.6 mmol) in DCM (200 mL) and added dropwise to a solution of 1,10-diaminodecane over a period of 2 h at room temperature prior to being stirred overnight at room temperature (RT). Subsequently, 1 M HCl (10 mL) was added to the reaction mixture and a white precipitate was formed. The solvent was removed by rotary evaporation and the white precipitate was washed several times with ethyl acetate.

Yield: 2.5 g, 69.5 % ^{1}H NMR (300 MHz, $CDCl_3$): δ (ppm)= 7.90 (br s, 3H), 7.41-7.25 (m, 5H), 5.02 (s, 2H), 3.02-2.95 (m, 2H), 2.79-2.72 (m, 2H), 1.57-1.50 (m, 2H), 1.42-1.26 (m, 14H). ^{13}C NMR (75 MHz, $CDCl_3$): δ (ppm) = 156.03, 137.29, 128.29, 127.68, 127.64, 65.01, 40.13, 38.73, 29.35, 28.82, 28.72, 28.64, 28.46, 26.92, 26.18, 25.76.

Synthesis of 4

Undecaethylene glycol methyl ether (0.591 g, 1.11 mmol) was first activated with CDI (0.222 g, 1.37 mmol) for 1h at RT (LCMS: t= 4.14 min, m/z: 611.27 $[M+H]^+$). Subsequently, diisopropylethylamine (DIPEA) (0.4 mL, 2.22 mmol) and **2** (0.460 g, 1.48 mmol) were added to the reaction mixture and refluxed overnight. When the reaction was complete (LCMS: t= 6.7 min, m/z: 670.5 $[M+H]^+$), the compound was purified by flash chromatography on a C18 silica column using a gradient of H_2O/CH_3CN 20-90% over 40 min. The solvent was removed *in vacuo* and the compound was lyophilized and isolated as white solid.

Yield: 0.336 g, 45%, ^{1}H NMR (300 MHz, $CDCl_3$): δ (ppm) = 7.36 – 7.23 (m, 5H), 5.06 (s, 2H), 4.22 – 4.13 (m, 2H), 3.62 (s, 47H), 3.56 – 3.45 (m, 3H), 3.35 (s, 4H), 3.13 (t, 5H), 1.47 – 1.39 (m, 4H), 1.25 (s, 13H). ^{13}C NMR (75 MHz, $CDCl_3$): δ (ppm) = 156.39, 136.73, 128.42, 127.96, 77.62, 77.19, 76.77, 71.88, 70.52, 70.45, 69.62, 66.40, 63.71, 58.93, 53.49, 41.03, 40.96, 29.88, 29.34, 29.14, 26.64. LCMS: t= 6.7 min, (m/z): 670.5 $[M+H]^+$.

Synthesis of 5

4 (0.483 g, 0.55 mmol) was dissolved in dry MeOH (5 mL) and Pd/C (0.029 g, 0.275 mmol) was added. The round bottom flask was put under argon atmosphere and Et_3SiH (3.5 mL, 40 mmol) was added dropwise and the reaction mixture was stirred overnight at RT. Subsequently, the catalyst was removed by filtration over celite and the solvent was removed under a stream of N_2 gas overnight. The compound was redissolved in $CHCl_3$ (20 mL) and 3,4-dibutoxy-3-cyclobutene-1,2-dione (0.096 mL, 0.45 mmol) and DIPEA (0.195 mL, 1.12 mmol) were added and stirred together overnight at RT. The product was purified by flash chromatography on a C18 silica column using a gradient of H_2O/CH_3CN 20-90 % over 40 min. The compound was obtained as white solid.

Yield: 0.346 g, 72.5%,^{1}H NMR (300 MHz, $CDCl_3$) δ (ppm) =6.74 (s, 1H), 4.71 (q, 2H), 4.20 (m, 2H), 3.71 – 3.49 (m, 44H), 3.36 (s, 3H), 3.13 (m, 2H), 1.76 (m, 2H), 1.60 (m, 2H), 1.33 – 1.23 (m, 12H), 0.96 (t, 3H). ^{13}C NMR (75 MHz, $CDCl_3$): δ (ppm) = 159.46, 77.51, 77.08, 76.66, 73.35, 71.90, 70.54, 69.65, 63.80, 58.72, 44.84, 40.98, 32.00, 29.89, 29.30, 29.12, 29.03, 26.63, 26.28, 18.62, 13.46. LCMS: t= 6.5 min, (m/z): 867.83 $[M+H]^+$, MALDI: (m/z): 889.456 $[M+Na]^+$.

Synthesis of 1

5 (0.240 g, 0.277 mmol) was dissolved in $CHCl_3$ (15 mL) and 1,7-diaminoheptane (0.012 g, 0.129 mmol) and DIPEA (0.063 mL, 0.360 mmol) were added to the reaction mixture and refluxed overnight. The compound was purified by flash chromatography on a C18 silica column using a gradient of H_2O/CH_3CN 20-90 % over 40 min. The solvent was removed in *vacuo* and the compound was lyophilized and obtained as a white solid.

Yield: 0.103 g, 46.5%. ^{1}H NMR (300 MHz, $CDCl_3$): δ (ppm) = 7.84 (s, 1H), 7.60 (s, 1H), 5.04 (s, 1H), 4.22 (t, 2H), 3.77 – 3.51 (m, 46H), 3.40 (s, 3H), 3.14 (d, 2H), 1.64 (d, 4H), 1.55 – 1.18 (m, 18H). ^{13}C NMR (75 MHz, $CDCl_3$): δ (ppm) = 169.13, 167.20, 158.79, 156.68, 77.44, 77.01, 76.59, 71.91, 70.58, 70.51, 70.48, 69.73, 63.80, 59.03, 44.77, 41.08, 31.09, 29.93, 29.41, 29.20, 26.72, 26.39. LCMS: t= 6.48 min, (m/z): 1716.30 $[M+H]^+$, MALDI: (m/z): 1736.553 $[M+Na]^+$.

Synthesis of 2

1 (0.061 g, 0.035 mmol) was dissolved in anhydrous acetonitrile (5mL) and pentathiodiphosphorus(V) acid-P,P′-bis(pyridinium betaine (0.311g, 0.805 mmol) was added. The reaction mixture was stirred overnight at RT. After the filtration, the compound was isolated by flash chromatography on a C18 silica column using a gradient of H_2O/CH_3CN 30-90 % over 30 min. The compound was obtained as a yellow solid.

Yield: 0.018 g, 30% ^{1}H NMR (500 MHz, $CDCl_3$) δ (ppm) = 8.85 (s, 1H), 8.60 (s, 1H), 5.02 (s, 1H), 4.23-4.21 (m, 4H), 4.16-4.12 (m, 5H), 3.67-3.54 (m, 84H), 3.39 (s, 6H), 3.17-3.13 (m, 4H), 1.76-1.68 (m, 7H), 1.52 – 1.24 (m, 34H). ^{13}C NMR (125 MHz, $CDCl_3$): δ (ppm) = 204.02, 203.57, 170.96, 170.88, 156.58, 77.37, 77.12, 76.86, 71.89, 70.58, 70.43, 70.38, 70.26, 69.89, 63.74, 59.12, 44.20, 43.46, 41.16, 40.50, 31.04, 29.98, 29.47, 29.42, 29.31, 29.17, 26.80, 26.43, 25.51. LCMS: t= 7.43 min, (m/z): 1780.28 $[M+H]^+$.

Synthesis of sulfo-Cy3 and sulfo-Cy5 dye-conjugated squaramide-based bolaamphiphiles

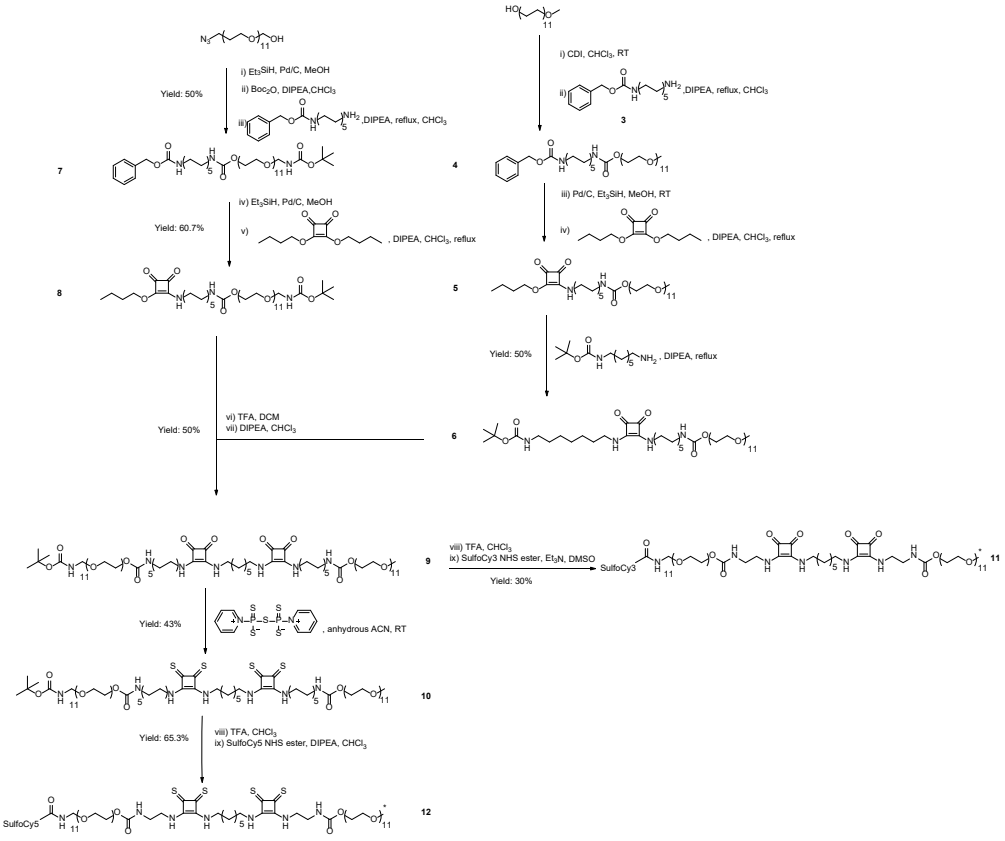

Synthesis of 6

5 (0.178g, 0.205 mmol) was dissolved in $CHCl_3$ (10 mL) with 1-boc-1,7-diaminoheptane (0.071g, 0.308 mmol) and DIPEA (0.107 mL,0.615 mmol) and the mixture was refluxed overnight. The compound was isolated by flash chromatography on a C18 silica column using a gradient of H_2O/CH_3CN 20-90 % over 30 min and was obtained as a yellowish solid.

Yield: 0.104 g, 50%. ^{1}H NMR (400 MHz, $CDCl_3$): δ (ppm) = 7.29 (s, 1H), 5.05 (s,1H), 4.71 (s, 1H), 4.19-4.15 (m, 2H), 3.63-3.50 (m, 46H), 3.18 – 2.98 (m, 3H), 1.83 – 1.70 (m, 1H), 1.64 – 1.53 (m, 3H), 1.45 (s, 9H), 1.32 – 1.20 (m, 15H). ^{13}C NMR (100 MHz, $CDCl_3$): δ (ppm) = 182.43, 168.05, 156.62, 77.39, 77.08, 76.76, 73.39, 71.94, 70.57, 69.66, 63.85, 59.02, 44.90, 44.59, 44.53, 41.03, 32.03, 31.17, 30.90, 30.63, 29.91, 29.36, 29.16, 29.05, 28.73, 28.47, 26.65, 26.43, 26.31, 18.65. LCMS: t= 6.67min. (m/z): MALDI: (m/z): 923.587 $[M+H\text{-}Boc]^+$, 1045.377, $[M+Na]^+$.

Synthesis of 7

O-(2-Azidoethyl)undecaethylene glycol (0.642 g, 1.12 mmol) was dissolved in anhydrous MeOH (10 mL) and Pd/C (0.059 g, 0.56 mmol) was added under N_2 atmosphere. Et_3SiH (3.57 mL, 22.4 mmol) was added dropwise to the reaction and stirred overnight. Subsequently, the compound was filtered over celite to remove the catalyst and the solvent was removed using a gentle stream of N_2 gas. Subsequently, the residue was redissolved in $CHCl_3$ (10 mL) in presence of DIPEA (0.585 mL, 3.36 mmol) and Boc_2O (0.404 g, 1.85 mmol) at room temperature. After 2 h hours, the product was confirmed by LCMS (t = 4.76 min, m/z: 545.78 $[M+H\text{-}Boc]^+$) and the solvent was removed from the oily residue prior to its activation with CDI (0.205 g, 1.23 mmol) at RT. After that the formation of the product was confirmed by LC-MS (t= 4.55 min, 639.17 m/z, $[M+H\text{-}Boc]^+$), the mixture was dissolved in $CHCl_3$ (10 mL) and the DIPEA (0.390 mL, 2.24 mmol) and N-Cbz-1,10-decanediamine (0.457g, 1.49 mmol) were added and refluxed overnight. The final compound was purified by flash chromatography on a C18 silica column using a gradient of H_2O/CH_3CN 20-90 % over 35 min and lyophilized. The final compound was obtained as a yellowish solid.

Yield: 50 % 0.483 g, ^{1}H NMR (400 MHz, $CDCl_3$): δ (ppm) = 7.31 – 7.16 (m, 5H), 4.99 (s, 2H), 4.11 (t, 2H), 3.56-3.42 (m, 66H), 3.54 (s, 11H), 3.23 – 3.18

(m, 2H), 3.11-3.01 (m, 4H), 1.42-1.35 (m, 17H), 1.22 – 1.15 (m, 13H). ^{13}C NMR (100 MHz, $CDCl_3$): δ (ppm) = 150.98, 77.53, 77.11, 76.69, 70.51, 70.24, 70.19, 69.64, 66.49, 63.73, 40.99, 29.90, 29.37, 29.17, 28.41, 26.67 LCMS: t=7.87 min, (m/z): 878.16 $[M+H]^+$.

Synthesis of 8

7 (0.410 g, 0.552 mmol) was dissolved in anhydrous MeOH (10 mL) and Pd/C was added under an N_2 atmosphere. Et_3SiH (1.76 mL, 11.04 mmol) was added dropwise and the reaction was stirred overnight. When the reaction was complete (LCMS: t = 3.65 min, m/z: 546.13 $[M+H]^+$) the compound was filtered over celite and the solvent was removed under a gentle stream of N_2 gas. The reaction mixture was dissolved was in $CHCl_3$ (5 mL) and DIPEA (0.192 mL, 1.1 mmol,) and squaric ester (0.095 mL, 0.442 mmol) were added. The reaction mixture was stirred overnight at RT and the product was purified by flash chromatography on a C18 silica column using a gradient of H_2O/CH_3CN 10-90 % over 40 min. The product was isolated as a yellowish solid.

Yield: 60.7 % 0.334 g, ^1H NMR (400 MHz, $CDCl_3$): δ (ppm) = 5.18 (s, 1H), 5.05 (s, 1H), 4.75-4.73 (t, 2H), 4.21-4.20 (t, 2H), 3.76-3.61 (m, 42H), 3.56-3.53 (m, 2H), 3.42-3.37 (m, 2H), 3.31 (s, 2H), 3.16-3.13 (m, 2H), 1.80-1.77 (m, 2H), 1.63-1.58 (m, 4H),1.49-1.45 (m, 15H), 1.31-1.28 (m, 12H), 1.00 – 0.86 (t, 3H) ^{13}C NMR (100 MHz, $CDCl_3$): δ (ppm) = 189.32, 184.23, 182.79, 177.23, 172.52, 156.43, 156.00, 79.01, 77.56, 77.24, 76.92, 74.25, 73.23, 70.50, 70.18, 70.13, 69.60, 63.73, 44.80, 40.95, 40.31, 31.98, 31.72, 30.60, 29.87, 29.32, 29.13, 29.03, 28.39, 26.63, 26.31, 18.61, 18.46, 13.59. LCMS: t=7.43 min, (m/z): 895.44 $[M+H\text{-}Boc]^+$, MALDI: (m/z): 896 m/z $[M+H\text{-}Boc]^+$.

Synthesis of 9

6 (0.028 g, 0.030 mmol) was deprotected using trifluoroacetic acid (TFA) (2 mL) stirring for 20 min at RT. After the removal of the acid using a gentle stream of N_2 gas, the compound was redissolved in $CHCl_3$ (10 mL), and **8** (0.024 mmol, 0.027 g) and DIPEA (2 eq, 0.060 mmol, 0.012 mL) were added. The mixture was refluxed overnight. The product was purified by flash

chromatography on a C18 silica column using a gradient of H_2O/CH_3CN 10-90% over 35 min and was obtained as a yellowish solid.

Yield: 0.0028 g, 50 %, ^{1}H NMR (400 MHz, $CDCl_3$): δ (ppm) = 7.92 (s, 1H), 7.66 (s, 1H), 4.22 (t, 4H), 3.68 (d, 89H), 3.61 – 3.53 (m, 4H), 3.34 (s, 3H), 3.16 (m, 6H), 1.65 (m, 7H), 1.49 – 1.25 (m, 49H). ^{13}C NMR (100 MHz, $CDCl_3$): δ (ppm) = 182.69, 181.76, 168.98, 167.34, 156.54, 77.38, 77.07, 76.75, 71.91, 70.57, 70.52, 70.26, 69.70, 63.78, 59.02, 44.73, 43.35, 41.08, 40.39, 31.19, 29.96, 29.47, 29.27, 29.24, 28.45, 26.75, 26.45, 24.97. LCMS: t=6.81 min, m/z: 1745.16 $[M+H\text{-}Boc]^+$, MALDI: (m/z): 1865.32 $[M+Na]^+$.

Synthesis of 10

9 (0.028 g, 0.015 mmol) was dissolved in anhydrous CH_3CN (3 mL) and pentathiodiphosphorus (V) acid-P,P′-bis(pyridinium betaine (0.133 g, 0.35 mmol) was added to the reaction mixture and stirred at RT overnight. Subsequently, the crude was filtered and purified by HPLC using a gradient of 30-90 % H_2O/ CH_3CN over 30 min. The acetonitrile was removed by rotary evaporation and the compound was lyophilized and isolated as a sticky yellow solid. Yield: 8 mg 30 % LCMS: t=8.00 min, m/z: 1809.83 $[M+H\text{-}Boc]^+$.

Synthesis of 11

9 (4.52 mg, 0.0023 mmol) was dissolved in TFA (1 mL) to remove the boc-protecting group and it was stirred for 10 min at RT. When the reaction was complete (LCMS: t= 5.77 min, m/z: 1745.27 $[M+H]^+$), the solvent was removed by a gentle stream of N_2 gas. The compound was redissolved in DMSO (1.5 mL) and Et_3N (200 µL) were added. Sulfo-Cy3 ester in DMSO (0.284 mL, 0.0028 mmol) was added and the reaction mixture was stirred overnight at RT. When the reaction was complete (LCMS: t=5.86 min, m/z: 2345.8 $[M+H]^+$), the solvent was removed by a stream of N_2 gas overnight. The compound was dialyzed for 2 days to remove the excess of dye, and purified by HPLC using a gradient of H_2O/CH_3CN 10-90 % over 30 min. The final compound was obtained as a sticky pink solid and was stored in the dark. Yield: 2.28 mg, 43 %, LCMS: t=5.86 min, m/z: 2345.8 $[M+H]^+$.

Synthesis of 12

10 (4.52 mg, 0.0023 mmol) was dissolved in TFA (1 mL) and stirred for 10 min at RT. When the reaction was complete (LC-MS: t=8.00 min, m/z: 1809.83 $[M+H]^+$), the solvent was removed by a gentle stream of N_2. The compound was redissolved in $CHCl_3$ (1 mL) and DIPEA (250 µL) was added. Subsequently, sulfo-Cy5 ester in DMSO (0.284 mL, 0.0028 mmol) was added and the reaction was stirred at RT for 3 h. When the reaction was complete (LCMS: t=6.86 min, m/z: 2435.20 $[M+H]^+$), the solvent was removed overnight by a stream of N_2 gas. The compound was dialyzed for 2 days to remove the excess of dye and HPLC purified using a gradient of H_2O/CH_3CN 10-90 % over 30 min. The final compound was obtained as a sticky blue solid and was stored in the dark. Yield: 3.77 mg, 65.3 % LCMS: t=6.86 min, m/z: 2435.20 $[M+H]^+$.

2.6.4 Characterization

Sample preparation

Supramolecular polymers

Monomers **1** and **2** were weighed independently and dissolved in milliQ water to obtain a 1 mM concentration of each monomer. Aliquots from the stock solutions were taken to prepare solutions at the desired concentration for solution phase measurements in water. All samples were equilibrated at RT overnight before measurement.

Supramolecular copolymers

To prepare supramolecular copolymers, stock solutions of **1** and **2** were first prepared independently. Monomer **1** was dissolved in HFIP (1 mM) and **2** in THF (1 mM) before removing the solvents using a gentle stream of N_2 gas. Subsequently, milliQ water was added to both compounds to obtain a final concentration of 1 mM for each stock. The solutions were then mixed in an equimolar ratio and diluted to the desired concentrations for measurement and equilibrated at RT overnight. A similar approach was used to prepare samples at different molar ratios.

UV-vis spectroscopy

UV-vis spectra of **1** and **2** and their copolymers were acquired on solutions (30 μM) prepared according to the sample preparation protocol described above. UV-vis spectra were recorded from 200-500 nm. Quartz cuvettes with a path length of 1 cm were used for measurements involving temperature or organic solvents (HFIP, DMSO or THF).

UV-vis titration

Supramolecular polymers of **1** and **2** (30 μM) were prepared using the preparation protocol described above. Monomer **1** (600 μL) was titrated with HFIP and **2** (600 μL) was titrated with THF (final volume: 652 μL) and a UV-vis spectra was recorded after the addition of each aliquot (2 μL) of organic solvent. The titration was stopped when a plateau in the absorbance was reached for each monomer. The degree of aggregation (α_{agg}) was plotted against the volume fraction of HFIP or THF in water and the experimental data were fitted with the equilibrium model described by Meijer[35] and co-workers and the thermodynamic parameters (ΔG°, σ, and m) were obtained in Maple software.

Table S1. Thermodynamic parameters for supramolecular polymerizations of **1** and **2**

	ΔG° (kJ/mol)	**m (kJ/mol)**	**σ**
1	-34	270	0.78
2	-35	200	0.06

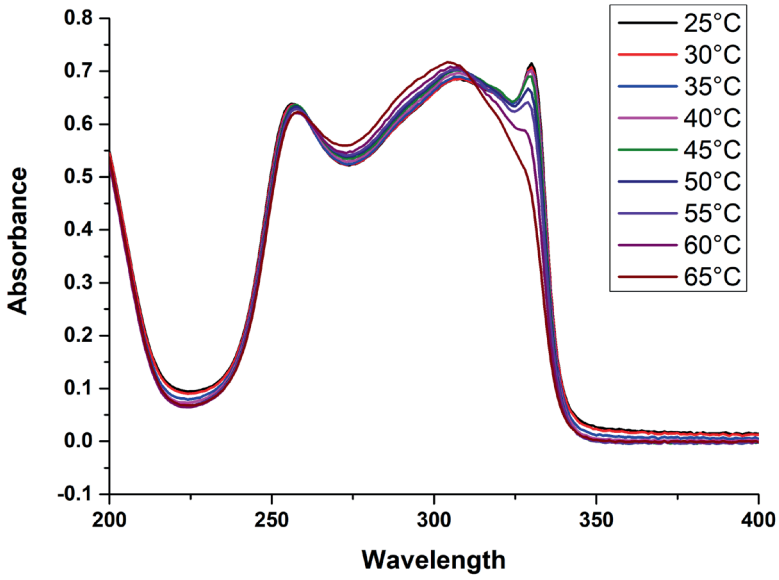

S2.1 Temperature-dependent UV-vis spectra of **1** (c=30 µM).

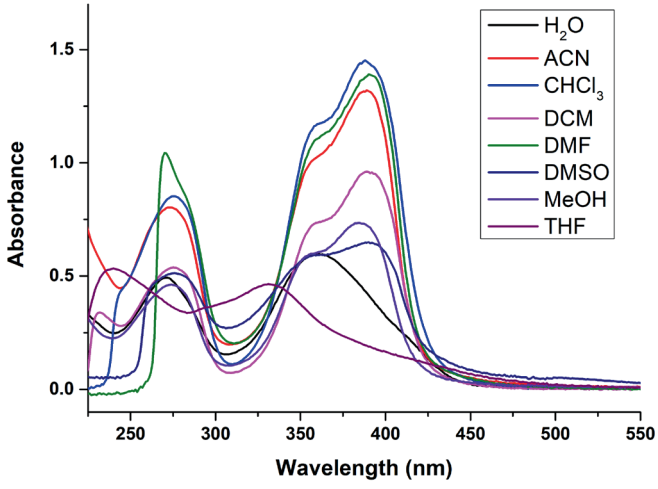

S2.2 UV-vis spectra of **2** (c=30 µM) in various organic solvents.

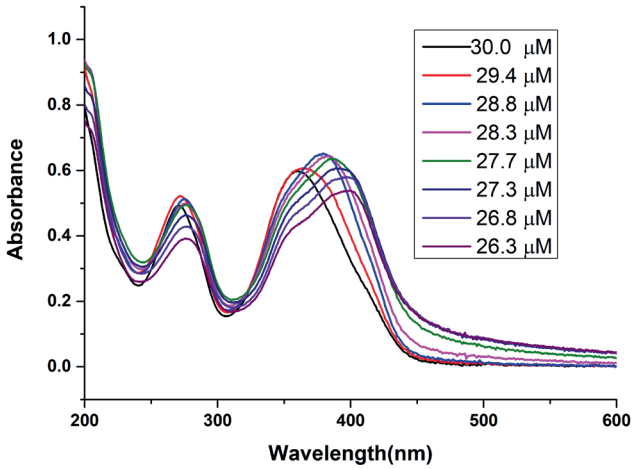

S2.3 UV-vis titration of **2** (c=30 μM) with HFIP.

Critical aggregation concentration (CAC) determination

A stock solution of **2** (1 mM) was prepared and diluted after overnight equilibration. Concentrations between 100 μM and 2 nM were prepared and then equilibrated for at least 3h. Each scattering measurement was carried out using a disposable DLS cuvette and performed in triplicate. The data was plotted using the scattering intensity as a function of log [C]. The critical aggregation concentration was then determined from the intersection of the two lines drawn through the points collected for the scattering intensities collected at the various concentrations.

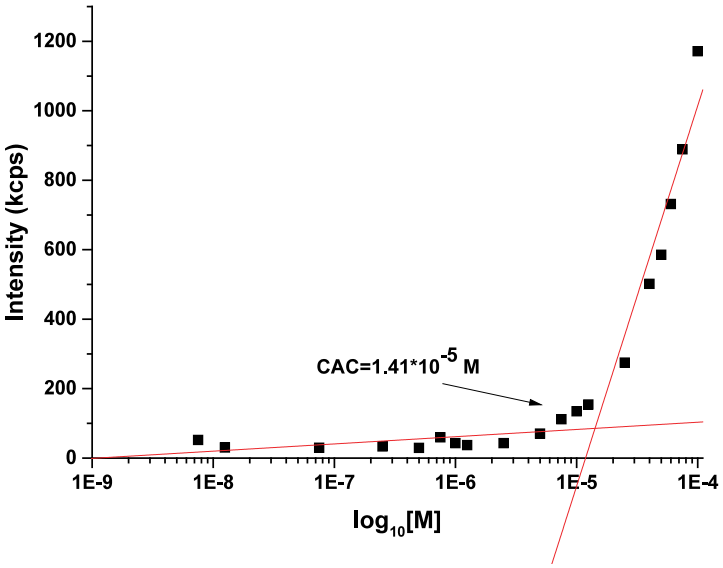

S2.4 Critical aggregation concentration determination of **2** using static light scattering.

Table S1: Static light scattering data of **1** and **2** in water, THF and HFIP (6 mM)

	Water (kcps)	**THF (kcps)**	**HFIP (kcps)**
solvent	-	1177.1	1506.9
2 (6 mM)	5077.7	1560.7	14871.5
1 (6 mM)	3831.6		3563.5

ζ–potential measurements

Solutions of **1** or **2** (1 mM) co-assembled with **11** or **12** (2 mol%) were prepared according to the protocol described above and equilibrated overnight. The samples were transferred to a ζ-potential dip cell prior the measurements.

Cryo-transmission electron microscopy (cryoTEM)

Two stock solutions were prepared by dissolving **1** in HFIP (3 mM) and **2** (3 mM) in THF. The organic solvents were removed by an N_2 stream and **1** was rehydrated with water and added to **2** to result in a 1:1 molar ratio and a final concentration of 580 μM**.** The sample was prepared applying 3 μL of the supramolecular (co)polymer solutions (5.8 mM) on to a freshly glow-discharged 300 mesh copper grid with a lacey-carbon support film (Electron Microscopy Sciences).

Calculation of persistence length (Pl) and bending rigidity (κ)

Cryo TEM images were converted in JPEG format and were analyzed by the Easyworm software. The fiber contour length was obtained by the copolymerization of oxo- and thiosquaramide. According to worm-like chain model (WLC), the persistence length was calculated from the mean end-to-end distance $\langle R^2 \rangle_{2D}$ of **1, 2** and the copolymers obtained by the copolymerization of **1** and **2** exploiting the following equation:

$$\langle R^2 \rangle_{2D} = 4P_l l \left[1 - \frac{2P_l}{l} \left(1 - e^{-\frac{l}{2P_l}} \right) \right]$$

Subsequently, the bending rigidity (κ) of the supramolecular polymer fibers was determined using this equation:

$$\kappa = K_b \cdot T \cdot P_l$$

where K_b is the Boltzmann constant, and T is the temperature expressed in K.

Forster resonance energy transfer (FRET) experiments

A solution of **1** (1 mM) in HFIP with 1 or 2 mol% of **12** was prepared and the solvent was removed by N_2 gas. Similarly, a solution of **2** (1 mM) in THF with 1 or 2 mol% of **11** was prepared and the solvent was removed. Water was added to both vials to obtain a final concentration of 1 mM for each stock and then mixed in an equimolar ratio. Aliquots from the mixed solutions were taken to prepare solutions at a 60 μM concentration and left to stand overnight. Fluorescence spectra were recorded using an Infinite M1000 Pro Tecan plate reader, using an excitation wavelength of 550 nm and measuring fluorescence emission from 570 to 800 nm.

^{1}H NMR spectra

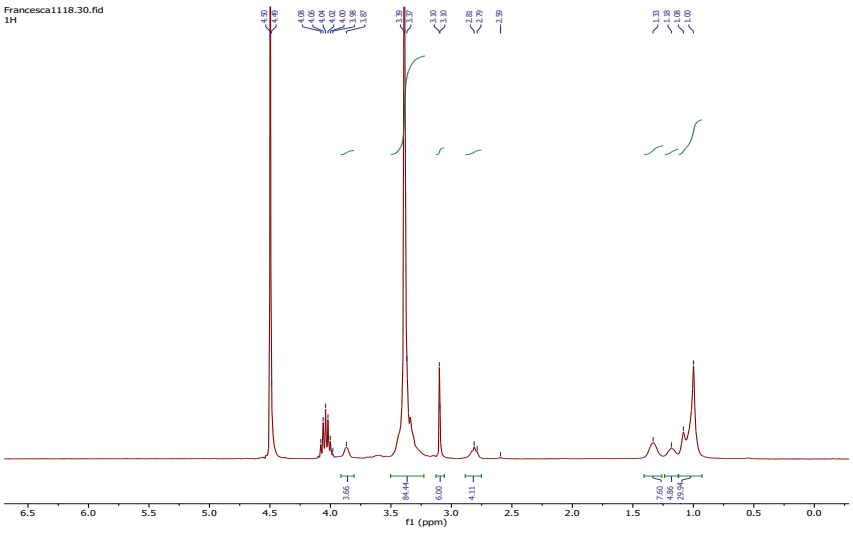

S2.5 ^{1}H NMR spectra of **1** (6 mM) in HFIP-d2

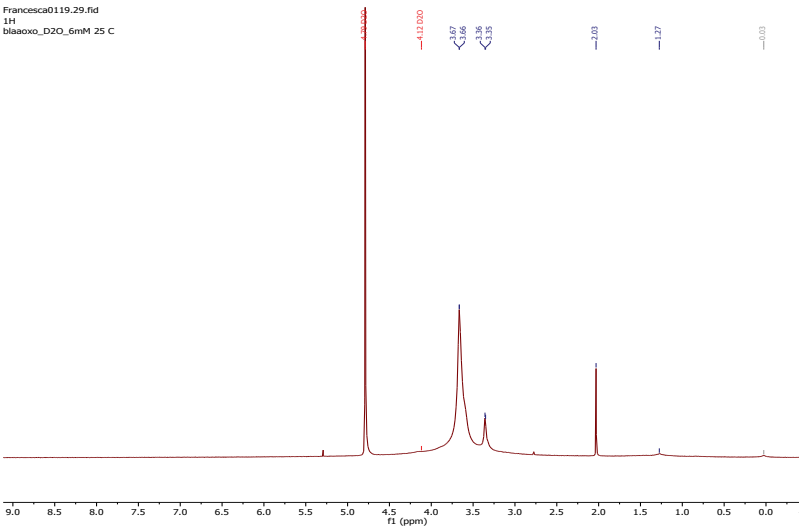

S2.6 ^{1}H NMR spectrum of **1** in D_2O (6 mM)

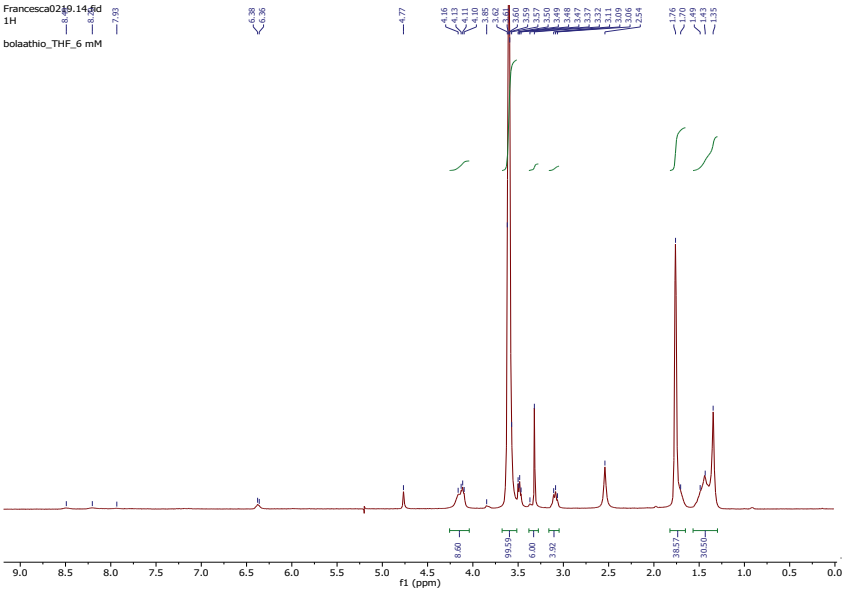

S2.7 ^{1}H NMR spectra of **2** in THF (6 mM)

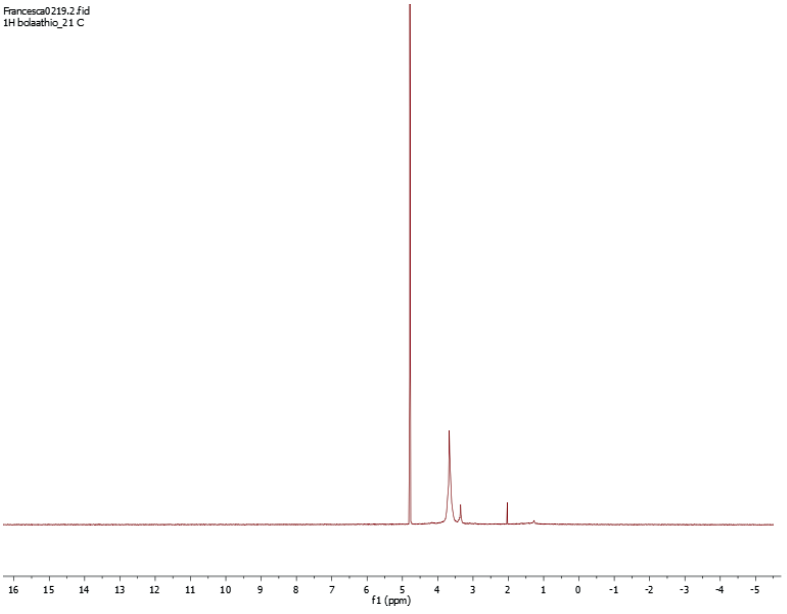

S2.8 ^{1}H NMR spectra of **2** in D_2O (6 mM).

Atomic force microscopy (AFM)

Solutions of **2** (30 µM) were independently prepared in H_2O, THF and HFIP and equilibrated overnight. An aliquot (25 µL) from each of these solutions was pipetted on a cleaved mica surface and dried overnight at RT before the measurements. The obtained AFM images were analyzed using the Nanoscope software.

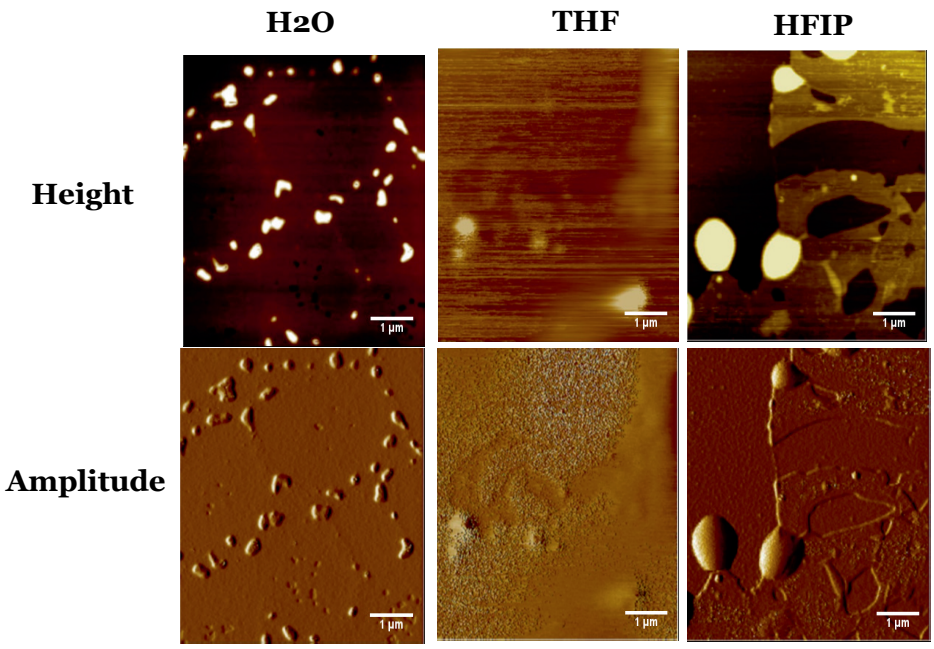

S2.9 AFM micrographs (height and amplitude) of **2** in water, THF and HFIP (15 µM), scale bar: 1 µm).